

Formation of nanoparticles during melt mixing a thermotropic liquid crystalline polyester and sulfonated polystyrene ionomers: Morphology and origin of formation

H.-S. Lee, Lei Zhu, R.A. Weiss*

Department of Chemical Engineering and Polymer Program, University of Connecticut, 97 N. Eagleville Road, Storrs, CT 06269-3163, USA

Received 27 May 2005; received in revised form 5 September 2005; accepted 9 September 2005

Available online 29 September 2005

Abstract

The formation of nanoparticles and the mechanism of their formation in a blend of a thermotropic liquid crystalline polyester (LCP) and the zinc salt of a lightly sulfonated polystyrene ionomer (Zn-SPS) were investigated using Fourier transform infrared (FTIR), thermogravimetric analysis (TGA), and gas chromatography–mass spectroscopy (GC–MS). Transmission electron microscopy (TEM) and wide-angle X-ray diffraction (WAXD) were used to study the morphology of the blends and structure of nanoparticles. The origin of nanoparticle formation appeared to be related to the development of phenyl acetate chain ends on the LCP that arose due to a chemical reaction between the LCP and residual catalytic amounts of zinc acetate and/or acetic acid that were present from the neutralization step in the preparation of the ionomer. Two-dimensional X-ray diffraction patterns for the blends revealed that chain-packing within nanoparticles was different than that of the LCP or the homopolymers prepared from the LCP co-monomers. The crystals formed in the nanoparticles were also stable to much higher temperature ($> 350\text{ }^{\circ}\text{C}$) than the parent LCP crystallites that melted at $\sim 280\text{ }^{\circ}\text{C}$.

© 2005 Elsevier Ltd. All rights reserved.

Keywords: Nanocomposites; Ionomer; Liquid crystalline polymer

1. Introduction

Composite materials attempt to combine the beneficial characteristics of two different materials to achieve physical and/or mechanical properties not found with one material alone. One such class of composites exploits the superior mechanical properties of liquid crystalline polymers (LCP) to reinforce another thermoplastic polymer. In practice, however, the properties of LCP/polymer composites fall far short of expectations, largely as a result of the poor interfacial adhesion between the dispersed microfibrillar LCP phase and the thermoplastic matrix phase. The best way to avoid problems induced by the interface between the rigid and flexible components is to disperse the rigid polymer at a molecular level; however, it is very difficult to achieve a molecular dispersion of rigid polymers in a blend with a flexible chain polymer. An alternative solution is to develop composites with the rigid or relatively rigid-rod polymer phase having nm-scale

dimensions, e.g. rods or fibers with diameters of the order of 10–50 nm.

Recently, we reported the formation of a nanoscale reinforcement as a result of melt-mixing a blend of the zinc salt of a sulfonated polystyrene ionomer (Zn-SPS) and a wholly aromatic, thermotropic, liquid crystalline polyester (LCP) at elevated temperatures [1]. The nanoparticles provided reinforcement of the ionomer comparable to what would be expected from short fibers with a modulus of at least 25 GPa. Various characterization techniques revealed that the nanoparticles possessed a unique structure and properties compared to those of the neat LCP. One objective of the current paper was to better characterize the morphology and structure of the nano-dispersed LCP phase produced by melt-mixing. Another objective was to ascertain the origin of the nanoparticle formation. One of the difficulties in characterizing the nanoparticles in the Zn-SPS/LCP blend was the insolubility of the LCP-phase, which precludes a number of useful analytical techniques, such as solution NMR and GPC. Therefore, the characterization of the Zn-SPS/LCP composites was limited to solid-state properties determined by transmission electron microscopy (TEM), wide-angle X-ray diffraction (WAXD)

* Corresponding author. Tel.: +1 860 486 4698; fax: +1 860 486 6048.

E-mail address: rweiss@mail.ims.uconn.edu (R.A. Weiss).

and Fourier transform infrared spectroscopy (FTIR). In addition, thermogravimetric analysis (TGA) and gas chromatography–mass spectroscopy (GC–MS) were used to determine the chemistry involved in the nanoparticle formation.

2. Experimental

2.1. Materials

The LCP used was Vectra A950 (Ticona Corp.; $T_m = 275\text{ }^\circ\text{C}$), a wholly aromatic thermotropic copolyester of 73% hydroxybenzoate (HBA) and 27% hydroxynaphthanoate (HNA). The ionomers used were the free acid derivative and zinc salt of lightly sulfonated polystyrene, SPS. SPS ionomers were prepared by sulfonation of a commercial atactic polystyrene, Styron 666 (Dow Chemical Co.; $M_n = 106,000$ and $M_w = 280,000$), in dichloroethane with acetyl sulfate in 1,2-dichloroethane at $60\text{ }^\circ\text{C}$ following the procedure of Makowski et al. [2]. This sulfonation process substitutes sulfonic acid groups randomly along the polystyrene chains and preferentially at the *para*-position of the phenyl ring. The sulfonation level was determined by titration of the sulfonic acid derivative, H-SPS, in a mixed solvent of toluene/methanol (90/10 v/v) with methanolic sodium hydroxide. The zinc salt was prepared by neutralizing the sulfonic acid derivative, H-SPS, in a 90/10 (v/v) toluene/methanol solution with a 20% excess of zinc-acetate (ZnAc). The nomenclature used for the ionomers is xyM -SPS, where xy and M denote the sulfonation level in mole percent and the cation, respectively. The ionomer salts were isolated from solution by precipitation into boiling deionized water, filtered, washed several times with deionized water and dried under vacuum.

Blends of SPS ionomers and LCP were prepared by melt mixing under a dry nitrogen atmosphere in a Brabender Plasticorder intensive mixer at $300\text{ }^\circ\text{C}$ using a 30 cm^3 mixing head with two counter-rotating rotors and a mixing speed of 30 rpm. Both polymers were dried at ca. $100\text{ }^\circ\text{C}$ for 24 h under vacuum prior to mixing. The LCP was first fluxed for 3 min and then the ionomer was added and mixed for an additional 13 min. Films of the neat polymers and blends were made by compression molding using a Carver hot press with a pressure of 10 ton. The blends were pre-heated to $300\text{ }^\circ\text{C}$ for 2 min, pressed for 5 min and then cooled to room temperatures by water circulation through the platens. The film thicknesses were ca. 0.5–1.0 mm.

2.2. Materials characterization

WAXD experiments were conducted on compression molded films in reflection mode, where one-dimensional (1D) data were collected with a Bruker D5005 X-ray powder diffractometer equipped with a scintillation counter detector and a Cu K_α radiation source ($\lambda = 0.1541\text{ nm}$) operating at a voltage of 40 kV and current of 40 mA. The scattering angle (2θ) was calibrated with silicon powder

($2\theta = 28.4^\circ$) and the data were corrected for background scattering. Other X-ray diffraction experiments were carried out at the Advanced Polymers Beamline (X27C, $\lambda = 0.1307\text{ nm}$) in the National Synchrotron Light Source (NSLS) at Brookhaven National Laboratory (BNL). In the 1D WAXD experiments, a linear position-sensitive detector (European Molecular Biological Laboratory, EMBL) was used with a sample-to-detector distance of ca. 10.0 mm. The scattering data from a silicon powder standard were used to calibrate the WAXD. 1D WAXD measurements were conducted during heating and cooling at a rate of $10\text{ }^\circ\text{C}/\text{min}$ in the temperature range between room temperature and $350\text{ }^\circ\text{C}$. Two-dimensional (2D) WAXD data were obtained with a Fuji imaging plate, equipped with a Fuji BAS-2500 scanner. Fiber-like Fraser corrections were performed on 2D WAXD patterns using Polar software (Stony Brook Technology and Applied Research, Inc.).

TEM was performed using a Philips EM300 transmission electron microscope operating at an accelerating voltage of 80 kV. Thin sections ranging from 100 to 200 nm thick were microtomed at room temperature with a Reichert-Jung Ultracut S ultramicrotome using a cutting speed of 1 mm/s. The sections were floated onto deionized water, collected on 300 mesh Cu/Pd grids and subsequently dried with filter paper. The sections were cut along the thickness direction of the compression molded film such that the electron beam was perpendicular to the thin part of the compression molded film. TEM images, typically 30k–40k in magnification for standard negative film, were electronically scanned and converted into grayscale TIFF image files. A quantitative image analysis of the particle sizes was performed by opening a digital file in Adobe Photoshop where the nanoparticles and/or LCP agglomerates were traced onto an overlapped blank layer. To ensure accurate measurements of the particle size, the image was sufficiently magnified so that most of the particles were counted. The resulting black/white layer file was imported into the image analysis program, Sigma Scan Pro v.5.0, which assigned each particle a numerical label and exported the particle's length to a separate file. Overall, 7–8 prints were analyzed for each sample, which provided ~ 1000 particles and good statistics for the analysis.

FTIR spectra were obtained with a Nicolet 560 Magna-IR spectrometer using a resolution of 2 cm^{-1} . The specimens for the FTIR experiments were prepared by either compression molding films or mixing the polymer with KBr powder. A total of 128 scans were averaged for each spectrum.

The thermal stability of the blends and neat polymers was studied using a Hi-Res TGA 2950 thermogravimetric analyzer (TA Instruments). Dynamic scans were obtained by heating the samples under either a nitrogen or air atmosphere from room temperature to $800\text{ }^\circ\text{C}$ at $10\text{ }^\circ\text{C}/\text{min}$. Isothermal scans were obtained by holding the sample at a fixed temperature, e.g. $300\text{ }^\circ\text{C}$, for 3 h.

Volatiles formed during the degradation of the blends and neat polymers were analyzed by combined GC–MS using a Hewlett Packard 5890 series II gas chromatograph with a mass

selective detector. A direct dynamic thermal desorption device, DTD, was installed at the top of the GC injection port. The DTD was used to thermally extract solid or liquid samples directly into the capillary column of the GC. The device allows a sample tube to be moved into and out of the injection port of the GC by controlled venting of the carrier gas within the capillary injection port. A small amount of the sample, ~ 0.2 mg, was sealed in a small glass tube by quartz wool, and the tube was transferred into the DTD and supported by a split vent purge flow of 300 mL/min. The injection port was preset at 300 °C and when the split vent purge flow was turned off, the sample tube fell into the injection port, initiating the experiment. The sample was isothermally annealed at the preset injection port temperature for 5 min and the volatiles formed passed into the GC column and were frozen by a liquid nitrogen trap. At the end of the isothermal annealing, the sample tube was ejected from the injection port by the vent purge flow and the liquid nitrogen trap was removed, which allowed for the analysis of the volatiles formed during the thermal annealing. That was accomplished by separating the volatiles by heating the GC column from 35 to 325 °C at a rate of 15 °C/min and analyzing the effluent with the MS.

3. Results and discussion

3.1. Morphology of Zn-SPS/LCP blends

A previous paper [1] showed that films of a 95/5 5.6Zn-SPS/LCP blend were optically transparent, while films of 85/15 5.6Zn-SPS/LCP blend were opaque. The difference in the optical properties of the two blends was a consequence of the dispersion and size of the LCP-domains, see Fig. 1. For the 95/5 5.6Zn-SPS/LCP blend, the LCP-phase was well-dispersed as rectangular prisms of ca. $30 \times 30 \times 150$ nm, too small to scatter visible light. In contrast, although similar nanoparticles formed in the 85/15 5.6Zn-SPS/LCP blend, some large domains with sizes of the order of micrometer remained. The opacity of the film of 85/15 blend was due to light scattering from the large domains, and the persistence of those large domains blends with higher LCP concentrations may be due to differences in the viscosity of the melts and/or that longer mixing times are needed to completely convert the macroscopic LCP-domains into nanoparticles.

Fig. 2 shows histograms of the particle lengths and pertinent statistical data obtained by image analysis using the TEM

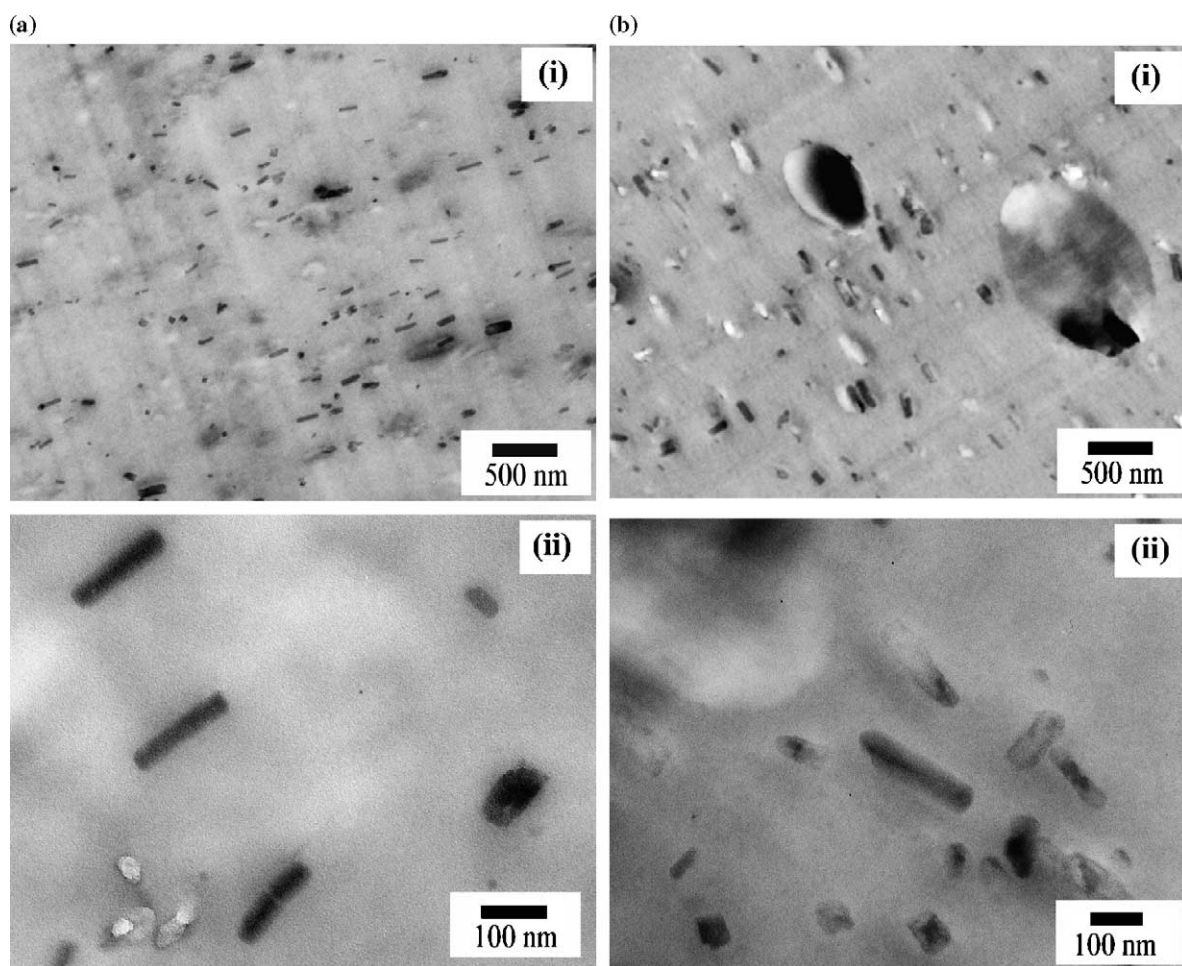


Fig. 1. (a) TEM micrographs for 95/5 (w/w) 5.6Zn-SPS/LCP blend mixed for 15 min at 300 °C in a Brabender mixer: (i) 20k magnification, (ii) 100k magnification; (b) TEM micrographs for 85/15 (w/w) 5.6Zn-SPS/LCP blend mixed for 15 min at 300 °C in a Brabender mixer: (i) 20k magnification; (ii) 80k magnification.

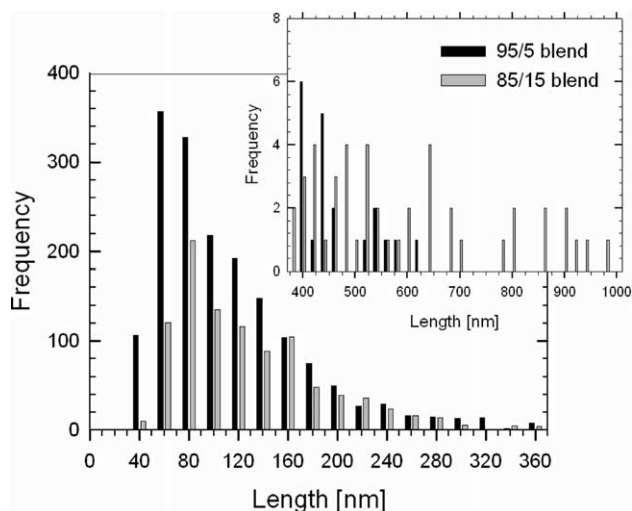


Fig. 2. Size distribution of particles measured from TEM images for 95/5 (w/w) 5.6Zn-SPS/LCP blend and 85/15 (w/w) 5.6Zn-SPS/LCP blend. The number and weight average particle lengths for the former blend were $\bar{\ell}_n = 106$ nm; $\bar{\ell}_w = 154$ nm determined from measurements of 1722 particles. For the latter blend, $\bar{\ell}_n = 147$ nm; $\bar{\ell}_w = 392$ nm determined from measurements of 1039 particles.

photomicrographs of the 95/5 and 85/15 5.6Zn-SPS/LCP blends. The number- and weight-average lengths of the nanoparticles for the 85/15 blend were significantly higher than those for the 95/5 blend. This result is due to the persistence of macroscopic LCP agglomerates in the former blend (see the graph insert showing the histograms for the larger particles), which is believed to be a consequence of the lower shear stresses in the 85/15 blend due to a lower melt viscosity compared to the 95/5 blend. The lower viscosity of the LCP melt tended to lower the blend viscosity. The area fraction occupied by discrete particles indicated that all of the LCP-phase was accounted for by the image analysis (if it is assumed that the nanoparticles in the compression-molded films were randomly oriented, the area fraction from the two-dimensional image is equivalent to the volume fraction of nanoparticles); the particle area fractions calculated for the 95/5 and 85/15 blends were 4.5 ± 0.6 and $13.0 \pm 2.0\%$, respectively. Those values compare well with the target volume percents of LCP (assuming densities for the Zn-SPS ionomer of 1.1 g/cm^3 [3] and the LCP of 1.4 g/cm^3) [4] of 4.0 and 12.2%, respectively.

The standard deviation of the area fraction for the 85/15 blend was considerably greater than for the 95/5 blend due to the error in accounting for the large LCP agglomerates, which in some cases were larger than the microtomed film thickness, i.e. ~ 200 nm. The particle density in the 95/5 5.6Zn-SPS/LCP blend, ca. $9.1 \text{ particles}/\mu\text{m}^2$, was nearly twice that in the 85/15 blend, $5.7 \text{ particles}/\mu\text{m}^2$, which reflects the higher degree of conversion of LCP macro-domains to nanoparticles in the former blend. That result is believed to be a consequence of the chemical reaction origin of the nanoparticles [1], which is discussed later in this paper, and the necessity of increasing the reaction time, i.e. the mixing time in the intensive mixer, as the LCP concentration of the composite increased.

3.2. Structure of the nanoparticles in the Zn-SPS/LCP composites

As described in the previous paper [1], the X-ray patterns for the Zn-SPS/LCP composites do not match the diffraction patterns for either the LCP or the homopolymers of its component monomers, hydroxybenzoate (HBA) and hydroxynaphthanoate (HNA). The crystalline form of homopoly(HBA) was identified by Lieser using electron diffraction [5]. At room temperature, the homopolymer has an orthorhombic unit cell ($a=0.75$ nm, $b=0.57$ nm, and $c=1.25$ nm) that was designated form I. A second polymorph, form II, was also seen at the room temperature for a low molecular weight specimen. Form II also has an orthorhombic unit cell ($a=0.38$ nm, $b=0.111$ nm, and $c=1.29$ nm). At elevated temperature, >290 °C, both crystals were converted to form III, which has an orthorhombic unit cell with dimensions of $a=0.92$ nm, $b=0.53$ nm, and $c=1.24$ nm. Form III is a pseudohexagonal ($a \approx \sqrt{3}b$) unit cell and has a lower calculated density than either form I or form II. Based on the WAXD, Yoon et al. [6] concluded that poly(HBA) has an orthorhombic unit cell with dimensions of $a=0.747$ nm, $b=0.567$ nm, and $c=1.255$ nm, which is consistent with the form I structure obtained by Lieser [5]. WAXD patterns for the poly(HNA) were studied by Iannelli and co-workers [7]; poly(HNA) has an orthorhombic cell with dimensions of $a=0.766$ nm, $b=0.598$ nm, and $c=1.712$ nm.

The structures of liquid crystalline copolymers based on HBA and HNA have been studied by several authors [8–10]. The X-ray patterns of a copolymer fiber show strong equatorial and non-periodic meridian reflections. For the 75/25 HBA/HNA copolymer, the structure obtained using an as-spun copolymer is analogous to the form III of the poly(HBA), and the thermal annealing leads to the generation of a structure analogous to form I of the poly(HBA) [11]. The values of the d -spacing and indices for reflections for the 95/5 5.6Zn-SPS/LCP blend, the LCP (75/25HBA/HNA copolymer) [11], poly(HBA) [6], and poly(HNA) [7] are listed in Table 1.

Fig. 3 shows a 2D WAXD image taken using a stretched fiber of the 95/5 5.6Zn-SPS/LCP blend. When a blend film was stretched, the nanoparticles oriented in the stretching direction and provided a fiber diffraction pattern for the structure analysis. An assumption made for this analysis was that the nanoparticles contained oligomer/polymer chains and the chains were highly oriented along the long axis of the nanoparticle. Sharp arcs were observed in the WAXD pattern for the stretched fiber. An orthorhombic unit cell was assumed in this analysis and the reflection arcs were assigned in Fig. 3. Based on these assignments and the d -spacing results in Table 1, the unit cell dimensions were proposed: $a=0.92$ nm, $b=0.654$ nm, and $c=1.240$ nm. These unit cell dimensions were close to those for poly(HBA) Form III. However, the relative intensities of the peaks for the nanoparticles are very different from those reported for the LCP and homopolymers in Table 1. This result indicates that the space group of the nanoparticles is different from that of the LCP and its homopolymers. To elucidate the detailed structure of

Table 1
The values of d -spacing for the 95/5 5.6Zn-SPS/LCP blend, LCP and its homopolymers

95/5 blend		75/25 HBA/HNA [62]		Poly(HBA) [60]		Poly(HNA) [61]	
$d_{\text{obs.}}$ (nm)	Position	d (nm)	hkl	d (nm)	hkl	d (nm)	hkl
0.920	Equator (100)	0.760	100 (0.8)	0.747	100 (1)	0.859	002 (4)
0.654	Equator (44)	0.570	010 (5.7)	0.628	002 (3)	0.773	100 (1)
0.520	Off-equator (62)	0.521	011 (1.9)	0.452	110 (100)	0.572	102 (3)
0.460	Equator (80)	0.447	110 (81.2)	0.425	111 (11)	0.471	110 (100)
		0.383	200 (48.3)	0.374	200 (42)	0.455	111 (4)
0.372	Off-equator (8)	0.313	210 (17.4)	0.314	004 (7)	0.430	004 (1)
0.310	Meridian (34)	0.304	211 (20.3)	0.307	113 (12)	0.413	112 (<1)
		0.269	120 (9.4)	0.303	211 (11)	0.382	200 (52)
0.307	Equator (9)	0.233	310 (17.8)	0.279	203 (2)	0.322	210 (1)
				0.265	120 (2)	0.317	211 (25)
				0.209	006 (5)	0.282	022 (1)
				0.195	304 (1)	0.234	310 (1)
				0.187	400 (1)	0.213	008 (2)

The number in parenthesis indicates the relative intensity of the peaks.

nanoparticles including unit cell dimensions and corresponding space group, a detailed study of the nanoparticle chemical structure is required.

3.3. Effect of temperature and annealing at elevated temperatures on the structure of Zn-SPS/LCP blends

Fig. 4 shows the changes in the WAXD profiles for the 85/15 5.6Zn-SPS/LCP blend during heating and cooling using a synchrotron radiation source. Because the diffraction patterns are quite noisy, it is difficult to locate the precise positions for each peak; however, various diffraction peaks can be identified by comparison of these patterns with the X-ray patterns discussed above. The peaks at $q=9.7 \text{ nm}^{-1}$ and $q=12 \text{ nm}^{-1}$ were only observed in the diffraction patterns for the blends; they were absent for the neat LCP. A peak at ca. $q=14 \text{ nm}^{-1}$

may be due to overlapped peaks at $q=13.7 \text{ nm}^{-1}$ ($d=0.460 \text{ nm}$) and $q=14.1 \text{ nm}^{-1}$ ($d=0.447 \text{ nm}$); the former is due to the blend and the latter is from the neat LCP (Table 1). The intensities of the peaks at $q=9.7 \text{ nm}^{-1}$ and $q=12 \text{ nm}^{-1}$ did not change with increasing temperature. In contrast, the intensity of the peak at $q=14 \text{ nm}^{-1}$ decreased as temperature increased. Despite the decrease in intensity, the reflection at $q=14 \text{ nm}^{-1}$ persisted at $350 \text{ }^\circ\text{C}$, even after 10 min annealing at that temperature. When the sample was cooled back to room temperature, the pattern became similar to that of the initial state. The X-ray diffraction pattern for the neat LCP at $290 \text{ }^\circ\text{C}$ shows only an amorphous halo [12,13]. Therefore, the remaining peak at $300 \text{ }^\circ\text{C}$, $\sim 14 \text{ nm}^{-1}$, was presumed to be a contribution from the nanoparticles. Similarly, the reflections at $q=9.7 \text{ nm}^{-1}$ and $q=12 \text{ nm}^{-1}$, which did not change upon heating or cooling, were attributed to the nanoparticles. The decrease in the intensity of the peak at $q=14 \text{ nm}^{-1}$ during heating is attributed to disappearance of the $q=14.1 \text{ nm}^{-1}$

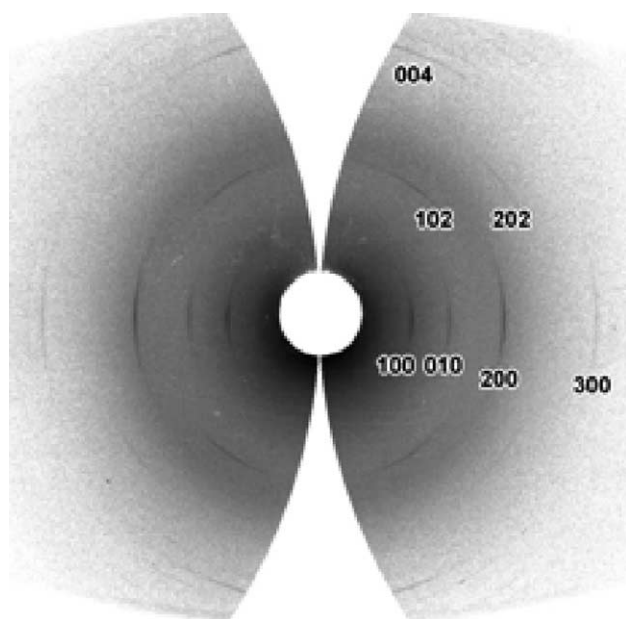


Fig. 3. Fraser corrected fiber pattern of the 95/5 (w/w) 5.6Zn-SPS/LCP blend. The fiber direction is vertical, and the intensity is in logarithmic scale.

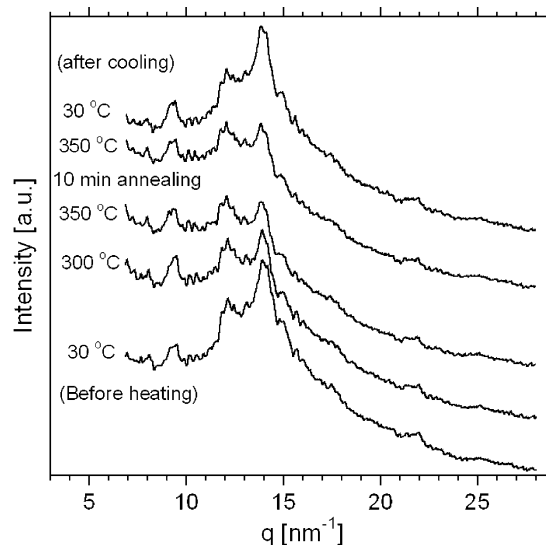


Fig. 4. Synchrotron WAXD profiles for 85/15 (w/w) 5.6Zn-SPS/LCP blend at various temperatures during heating and cooling.

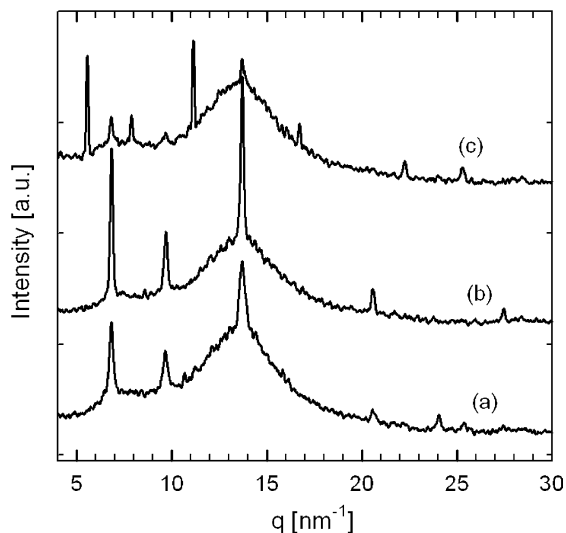


Fig. 5. Reflection mode WAXD profiles for 95/5 (w/w) 5.6Zn-SPS/LCP blend (compression-molded) annealed for 30 min at (a) 200 °C (b) 250 °C and (c) 300 °C.

contribution to that reflection, which represents the melting of large LCP domains. The molten LCP domains recrystallized during cooling, as evidenced by an increase in intensity and area of the peak at $q=14 \text{ nm}^{-1}$. It is notable that the nanoparticles did not melt at temperatures $<350 \text{ °C}$, which is well above the melting temperature of the neat LCP, $\sim 275 \text{ °C}$.

Fig. 5 shows the 1D reflection WAXD patterns for compression-molded films of the 95/5 5.6Zn-SPS/LCP blend that were annealed for 30 min at 200, 250 and 300 °C. Note that only the equatorial reflections shown in Fig. 3 were observable, since the data were collected in reflection mode. The annealed samples at 200 and 250 °C showed similar diffraction patterns, i.e. sharp peaks at $q=6.8$ ($d=0.920 \text{ nm}$), 9.6 ($d=0.654 \text{ nm}$) and 13.7 nm^{-1} ($d=0.460 \text{ nm}$), which were nearly identical with the profiles obtained from the samples melt-pressed for a relatively short time ($\sim 5 \text{ min}$) at 300 °C. The WAXD pattern for the composite film after annealing for 30 min at 300 °C, however, indicates that some structural changes occurred during annealing. New peaks at $q=5.54$ ($d=1.134 \text{ nm}$), 7.87 ($d=0.798 \text{ nm}$), 11.14 ($d=0.564 \text{ nm}$), 16.76 ($d=0.375 \text{ nm}$), and 22.28 nm^{-1} ($d=0.282 \text{ nm}$) were observed, while, the peaks at $q=6.8$, 9.6 , 13.7 , and 20.5 nm^{-1} still persisted but decreased in intensity. That result indicates that the annealing temperature had a significant effect on the chain structure and/or the chain-packing of the nanoparticles in the Zn-SPS/LCP blends. Interestingly, the new peaks that occurred for the sample annealed for 30 min at 300 °C showed the same ratios in peak position as the ratios for the un-annealed sample, but the position of the peaks shifted to lower q , i.e. larger d -spacing value.

In contrast, the unit cell of the nanoparticles appears to remain unchanged upon heat treatment. The relative intensity of the new peaks increased as annealing time increased; see Fig. 6(d) and (e). The values of q and the d -spacing obtained from powder diffraction profiles for the 95/5 5.6Zn-SPS/LCP

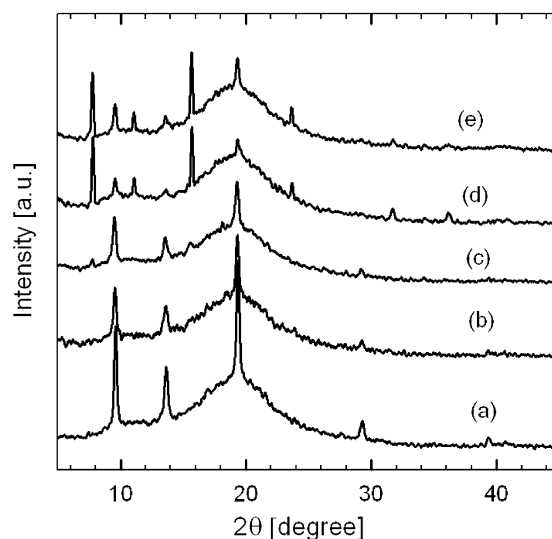


Fig. 6. Reflection mode WAXD profiles for 95/5 (w/w) 5.6Zn-SPS/LCP blend (compression-molded) annealed at 300 °C for (a) 5 min, (b) 10 min, (c) 20 min, (d) 30 min and (e) 60 min.

blends annealed for various times are listed in Table 2. The synchrotron X-ray study on this system indicated that the diffraction peaks at $q=9.70$ and 13.72 nm^{-1} persisted up to at least 350 °C, and no significant change was detected in either the intensity or the position of the peaks even after 10 min of annealing at 350 °C; see Fig. 4.

Fig. 7 shows the 2D WAXD patterns for a stretched fiber of a 95/5 5.6Zn-SPS/LCP blend annealed for 30 min at 300 °C. Surprisingly, all of the sharp peaks appeared at the equator in the 2D pattern, while the 2D WAXD pattern of a stretched fiber of the un-annealed 95/5 5.6Zn-SPS/LCP blend showed a strong off-axis peak in the scattering pattern, which is indicative of three dimensional ordering of chains [11]. The absence of meridional and quadrant peaks in the annealed sample indicates that the crystal structure changes and the total unit cell dimensions are difficult to solve since all the reflections are on the equator and no c -axis information can be obtained.

To ensure that the origin of the WAXD changes was related to the nanoparticles and not changes in the structure of the ionomer or LCP, the neat LCP and Zn-SPS were annealed for various times at 300 °C to ascertain any changes in their WAXD due to the exposure to elevated temperatures. Fig. 8(a) shows the powder diffraction patterns for 5.6Zn-SPS un-annealed and annealed for 30 min at 300 °C. Annealing at 300 °C had no effect on the WAXD pattern. Similarly, films of the LCP were also annealed at 300 °C for various times; see Fig. 8(b). Although there were some minor changes in the WAXD patterns upon annealing the LCP, those changes were consistent with the effect of annealing the LCP reported in the literature [9,11], i.e. the change in the crystalline structure from orthorhombic to pseudo-hexagonal. These results confirmed that the changes in the WAXD patterns observed for the ionomer/LCP composites discussed above were due to the formation of the nanoparticles.

Table 2
The values of d -spacing and q for the 95/5 5.6Zn-SPS/LCP blends annealed for various times at various temperatures

Annealing temperature/time	d -spacing [nm] (q [nm^{-1}])								
200 °C/30 min	0.924 (6.80)			0.650 (9.67)		0.458 (13.72)		0.305 (20.60)	0.261 (24.07)
250 °C/30 min	0.922 (6.81)			0.649 (9.68)		0.458 (13.72)		0.305 (20.60)	0.229 (27.44)
300 °C/5 min	0.919 (6.84)			0.648 (9.69)		0.458 (13.72)		0.305 (20.60)	0.229 (27.44)
300 °C/20 min	1.143 (5.50)	0.929 (6.76)		0.652 (9.64)	0.570 (11.02)	0.460 (13.66)		0.306 (20.60)	
300 °C/30 min	1.134 (5.54)	0.924 (6.80)	0.798 (7.87)	0.649 (9.68)	0.564 (11.14)	0.458 (13.72)	0.375 (16.76)	0.282 (22.28)	0.248 (25.34)
Proposed (hkl)	(100)*	100	(010)*	(010)	(200)*	(200)	(300)*	(300)	(400)*

The proposed (hkl) are based on the tentative orthorhombic unit cell: $a=0.920$ nm, $b=0.654$ nm, and $c=1.240$ nm for the nanoparticles. Unit cell dimensions of $a=1.134$ nm and $b=0.798$ nm are suggested on the basis of tentative (hkl)* for newly emerged peaks upon annealing more than 30 min at 300 °C. Again, since the WAXD was in reflection mode, only reflections on the equator were observed and listed in this table.

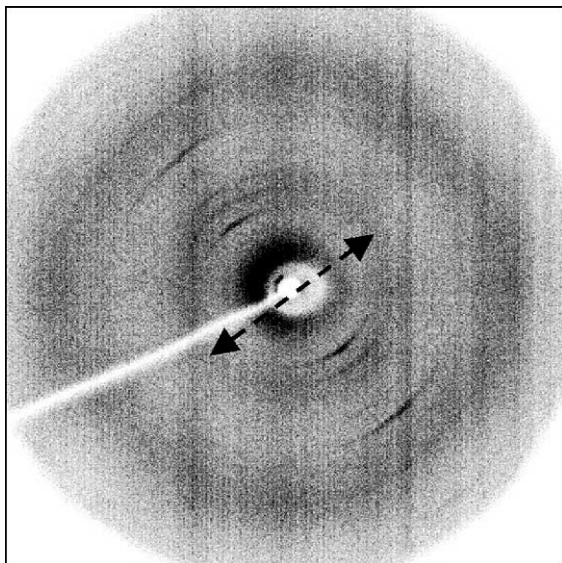


Fig. 7. Two-dimensional (2D) WAXS pattern for 95/5 (w/w) 5.6Zn-SPS/LCP blend stretched fiber annealed at 300 °C for 30 min. The arrow indicates a fiber direction.

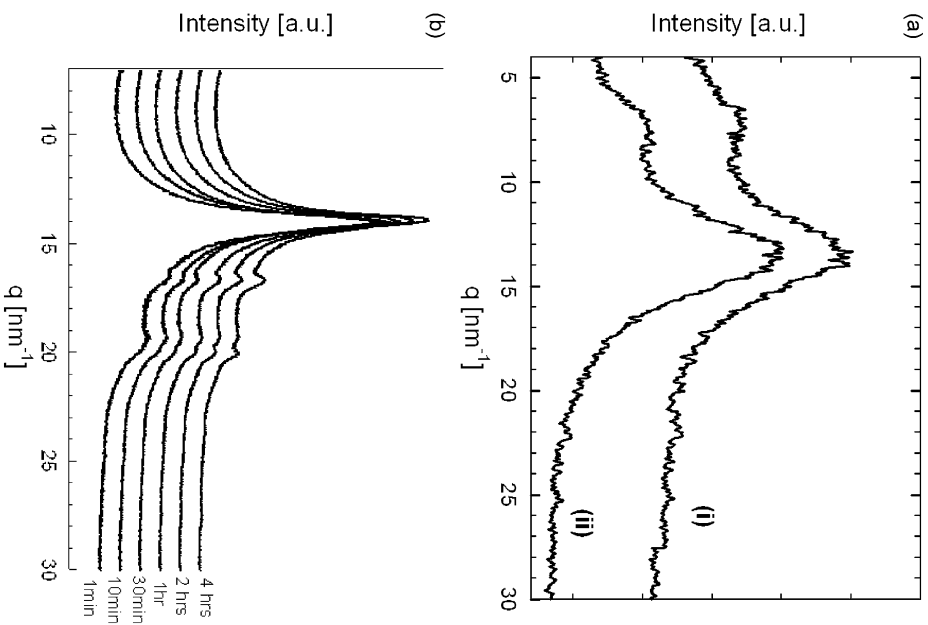


Fig. 8. WAXD profiles for (a) pure 5.6Zn-SPS; (i) un-annealed (ii) annealed at 300 °C and (b) the LCP annealed at 300 °C for various time periods.

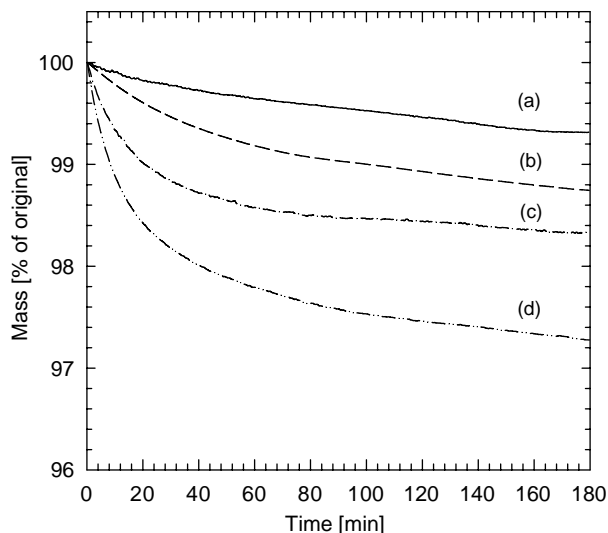


Fig. 9. Thermogravimetric curves for 5.6Zn-SPS/LCP blends and neat polymers under isothermal condition at 300 °C; (a) LCP, (b) 5.6Zn-SPS, (c) 95/5 and (d) 85/15 5.6Zn-SPS/LCP blends.

3.4. Thermal stability of Zn-SPS/LCP blends: TGA and GC-MS studies

Isothermal TGA thermograms obtained at 300 °C for the 5.6Zn-SPS, LCP and the blends are shown in Fig. 9; 300 °C was chosen because the blending and preparation of the film were performed at that temperature. Because that temperature was a harsh condition, especially for the Zn-SPS ionomer, one might expect that considerable degradation of the two polymers may have occurred during melt blending that may have contributed to the formation of the nanoparticles. However, the mass loss of the neat Zn-SPS and LCP after 20-min at 300 °C was actually quite small; the mass loss for the Zn-SPS and LCP were 0.40 and 0.18%, respectively. The time of 20 min was comparable to the residence time of the blend melt in the mixer during blending. Even after 3 h at 300 °C, the mass loss was less than ca. 1% for both neat polymers. Still, that small mass loss could represent a significant amount of polymer degradation, depending on what was the degradation mechanism.

The isothermal TGA thermograms for the 95/5 and 85/15 5.6Zn-SPS/LCP blends showed a larger mass loss than that for the individual polymer components, indicating lower thermal stability of the blends compared with the neat polymers. Fig. 10 plots the relative mass loss vs. time at 300 °C for the blends during the isothermal TGA experiment, where the data for the blends were normalized by the sum of the mass loss of the two neat polymers (i.e. $0.95 \times (\text{Zn-SPS})_{\text{deg}} + 0.05 \times (\text{LCP})_{\text{deg}}$ for the 95/5 blend and $0.85 \times (\text{Zn-SPS})_{\text{deg}} + 0.15 \times (\text{LCP})_{\text{deg}}$ for the 85/15 blend, where $(\text{Zn-SPS})_{\text{deg}}$ and $(\text{LCP})_{\text{deg}}$ are mass losses for the neat ZnSPS and LCP, respectively). For short exposure times to 300 °C, the amount of mass loss for the blend was considerably higher than the sum of mass losses for the neat LCP and Zn-SPS, indicating that degradation of the blends was accelerated by some interaction between the polymers. With increasing time, however, the amount of mass loss of

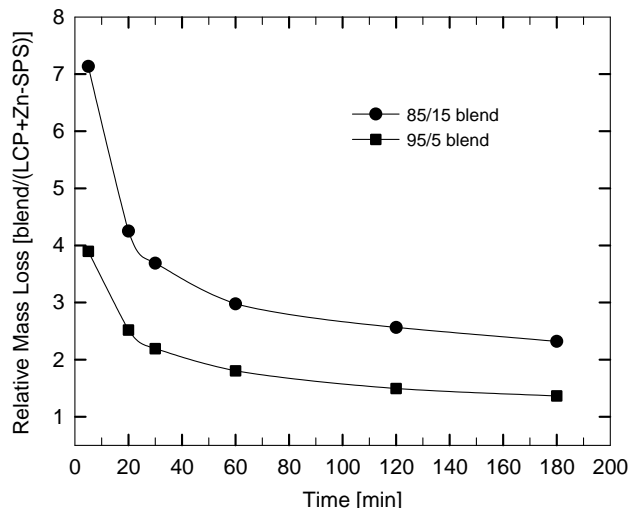


Fig. 10. The ratio of the amount of degraded products of the 5.6Zn-SPS/LCP blends with the summation of amount of volatiles of two neat polymers at certain times during isothermal TGA experiment at 300 °C.

the blend was comparable or slightly higher than that of the sum of the two components.

Fig. 11 shows representative GC-MS results for the neat Zn-SPS, LCP and their blends after annealing at 300 °C for 5 min. For the Zn-SPS, the major degradation product formed was styrene. No peak for SO₂ was found in the GC-MS result, indicating that very little or no desulfonation of the sulfonate groups occurred in the Zn-SPS, which is consistent with previous studies of the degradation of sulfonated polystyrene [14,15]. The major degradation product for the LCP was phenol, which is in agreement with reports in the literature for the degradation of this particular LCP [16–19]. A small peak for acetic acid was also observed in Fig. 11(a), which was due to residual zinc acetate (ZnAc) from the neutralization step in the preparation of the Zn-salt of the ionomer. The ZnAc can be removed by solvent extraction for long times with methanol, but this becomes problematic when large quantities of the ionomer are produced, e.g. as were necessary in this research for melt-mixing blends in a Brabender mixer. In that case, very long times, ~40 h, and large quantities of solvent were needed to reduce the ZnAc residue to <200 ppm [1,20]. Since the residual ZnAc appears to be responsible for the formation of the nanoparticles [1], it was fortuitous that the failure to adequately remove the neutralizing agent for the ionomer actually provided the means for forming the nanoparticles.

The GC-MS results for the blends, Fig. 11(c) and (d), were noticeably different than the results for the neat polymer components. A number of volatiles other than styrene and phenol were identified during the degradation of the blends, though phenol was still the major degradation product for both blends. The other volatiles identified in both blends were phenyl acetate, *o*-acetyl phenol, 4-hydroxy benzoic acid, and 3-phenyl furan. Among those volatiles, phenyl acetate and *o*-acetyl phenol are likely to originate by the reactions of the acetate group and/or acetic acid with a phenyl ring having a hydroxyl group or ester group. However, it is also possible that

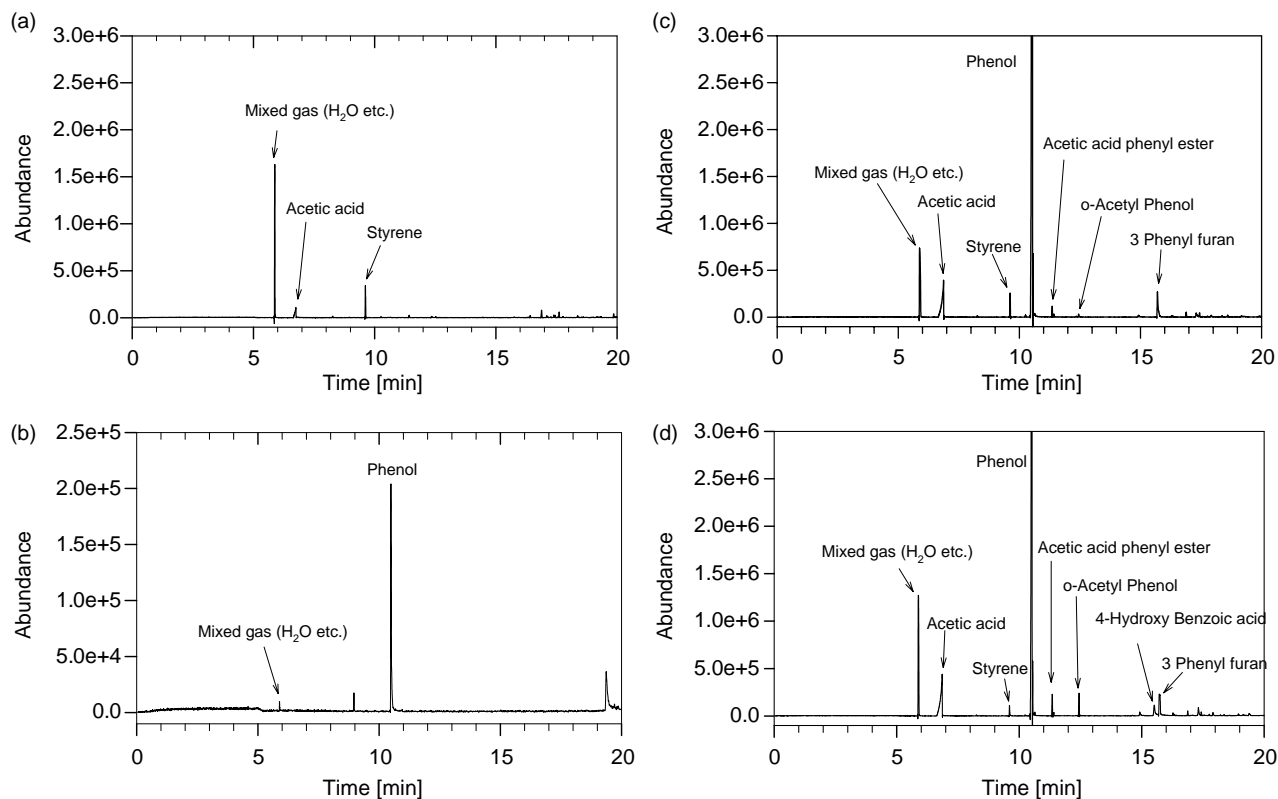


Fig. 11. Representative GC–MS results annealed at 300 °C for 5 min: (a) 5.6Zn-SPS, (b) LCP, (c) 95/5 5.6Zn-SPS/LCP and (d) 85/15 5.6Zn-SPS/LCP blends.

phenyl acetate and *o*-acetyl phenol were generated by the reaction of an acetate group and/or acetic acid with phenol, since phenyl acetate and *o*-acetyl phenol can be produced from phenol with the proper catalyst. Zinc salts (e.g. ZnAc [21], zinc benzoate [22], and zinc acetylacetonate [23]) are known catalysts in the condensation reaction or ester exchange reaction in polyesters. So, perhaps, ZnAc and/or zinc sulfonate group catalyzed the reaction with phenol.

Although the above explanation for the formation of the phenyl acetate and *o*-acetyl phenol molecules may be feasible, there is another explanation that is consistent with the FTIR results discussed later in this paper. In wholly aromatic polyesters with the structure $\phi_1\text{-CO-O-}\phi_2$, the C–O bonds between CO–O are preferentially cleaved over the C–O bonds between O– ϕ_2 , and the C–C bonds between $\phi_1\text{-CO}$ are preferentially cleaved over the other types of C–C bonds [24, 25]. Figs. 12 and 13 illustrate the possible pathways for the degradation of the LCP in the presence of acetic acid based on the degradation products detected by GC–MS. The scheme in Fig. 12 explains the formation of phenyl acetate and 4-hydroxy benzoic acid. The possible pathways to form phenol and *o*-acetyl phenol are presented in Fig. 13. A zinc catalyst can react with phenyl acetate to form *o*-acetyl phenol [26], which lends some credence to the formation of *o*-acetyl phenol from the phenol acetate end groups of the LCP. The formation of 3-phenyl furan appears to be related to the naphthanonic group in the LCP; however, the detailed pathway of its formation is not yet clear.

The GC–MS study of the degradation of the Zn-SPS/LCP blends suggests that chains of the LCP can be modified by chain scission and subsequent reactions that involve either acetic acid and/or ZnAc during annealing at 300 °C. The chains with modified end groups may crystallize in a different way from that of the neat LCP, which would explain the changes in the crystalline structure measured by WAXD. Because the major degradation product identified by GC–MS for the blends was phenol, it seems unlikely that the chain sequence changed much in the nanoparticles, but that the major difference between the nanoparticle structure and the original LCP may simply be the end groups and the molecular weight.

3.5. FTIR analysis of the Zn-SPS/LCP blend

Because of its sensitivity to the changes in the local environment of specific groups along the polymer chain, FTIR can provide information about the chain modification (e.g. chemical reaction, degradation, etc.). Distinct changes in the spectra of the blends were observed in the regions of the carbonyl stretching ($1750\text{--}1680\text{ cm}^{-1}$) and carbon–carbon (C–C) skeletal stretching in the aromatic ring ($1600\text{--}1300\text{ cm}^{-1}$). Changes in the bands specific for the sulfonate groups were difficult to resolve, because of overlapping bands from other chemical species.

Fig. 14 shows the carbonyl stretching and C–C stretching region of the FTIR spectra for the 5.6Zn-SPS/LCP blends and the neat component polymers. A small shift of the carbonyl

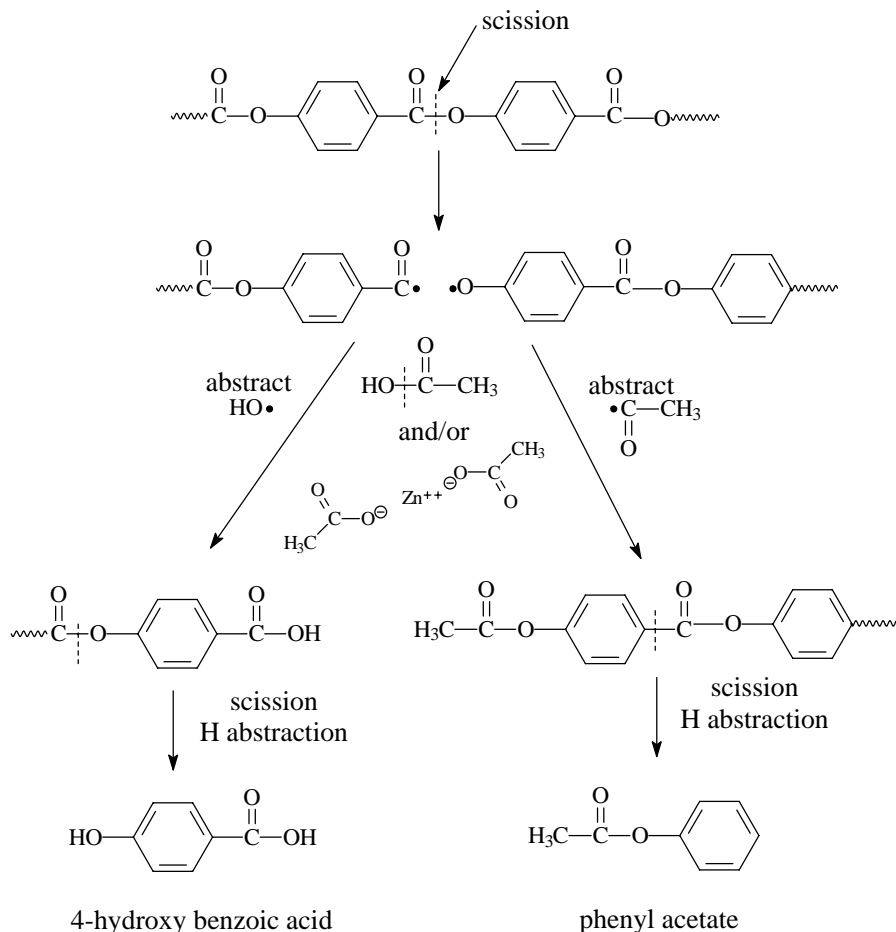


Fig. 12. Proposed mechanism of degradation process of the LCP in Zn-SPS/LCP blend: formation of 4-hydroxyl benzoic acid and phenyl acetate.

stretching band of the LCP to higher frequency, from 1735 to 1743 cm^{-1} , was observed for the 95/5 and 85/15 blends, though the shift was much clearer for the 95/5 blend. If the carbonyl group were involved in an interaction with another functional group, the strength of carbonyl stretching should weaken and the band should shift to lower frequency. However, the trend observed for the blends was in the opposite direction, i.e. a blue-shift. The degradation mechanism proposed in Fig. 12, specifically the formation of phenyl acetate end groups, may provide a clue for this result. The shift of the carbonyl stretching band can be explained by the presence of an acetate end group. The carbonyl stretching of phenyl acetate normally appears at a frequency of $\sim 1765\text{ cm}^{-1}$, due to conjugation involving the single-bonded oxygen [27], which is higher than the frequency observed for the blends, 1743 cm^{-1} . The close chain-packing within the nanoparticles may induce intermolecular hydrogen bonding with hydroxyl end groups of other chains, which lowers the strength of the carbonyl band, and so the shift to higher frequency is less than it would be for phenyl acetate.

The change of carbonyl stretching in the FTIR spectra for the 85/15 blend is somewhat different from that for the 95/5 blend. The carbonyl stretching band for the 85/15 blend was asymmetric in shape, which suggests overlapping absorptions: one arising from the LCP (1735 cm^{-1}), and the other caused

by the acetate end groups involved with the formation of nanoparticles (1743 cm^{-1}). The differences between 95/5 and 85/15 blends in the FTIR spectra seem to arise from differences in the degree of conversion of the LCP to nanoparticles and may be related to the morphology of the two blends discussed earlier in this paper. For the 95/5 blend, in which most of the LCP was converted to nanoparticles, the carbonyl stretching band appeared to be shifted; whereas, the compound absorbance of the carbonyl peak was observed for the 85/15 blend, in which both large LCP agglomerates and nanoparticles existed. The correspondence of the infrared spectrum, the morphology and the proposed degradation mechanism lends credence to the conclusions that degradation of the LCP is responsible for the nanoparticle formation and that changes in the carbonyl absorption in the infrared spectrum can be used to monitor the formation of nanoparticle.

In addition to the carbonyl stretching band at 1743 cm^{-1} , another band appeared in the region of $1680\text{--}1690\text{ cm}^{-1}$ for the blends. That peak may arise from three possible sources: (1) acetic acid, (2) end-groups containing carboxylic acid or (3) acetyl or hydroxyl end-groups. The carbonyl stretching for benzoic acid and *o*-acetyl phenol occurs at 1680 cm^{-1} due to hydrogen bonding [27]. Although the absorption of the carbonyl of acetic acid may also occur at a similar frequency, the band at 1685 cm^{-1} is more likely caused by modified

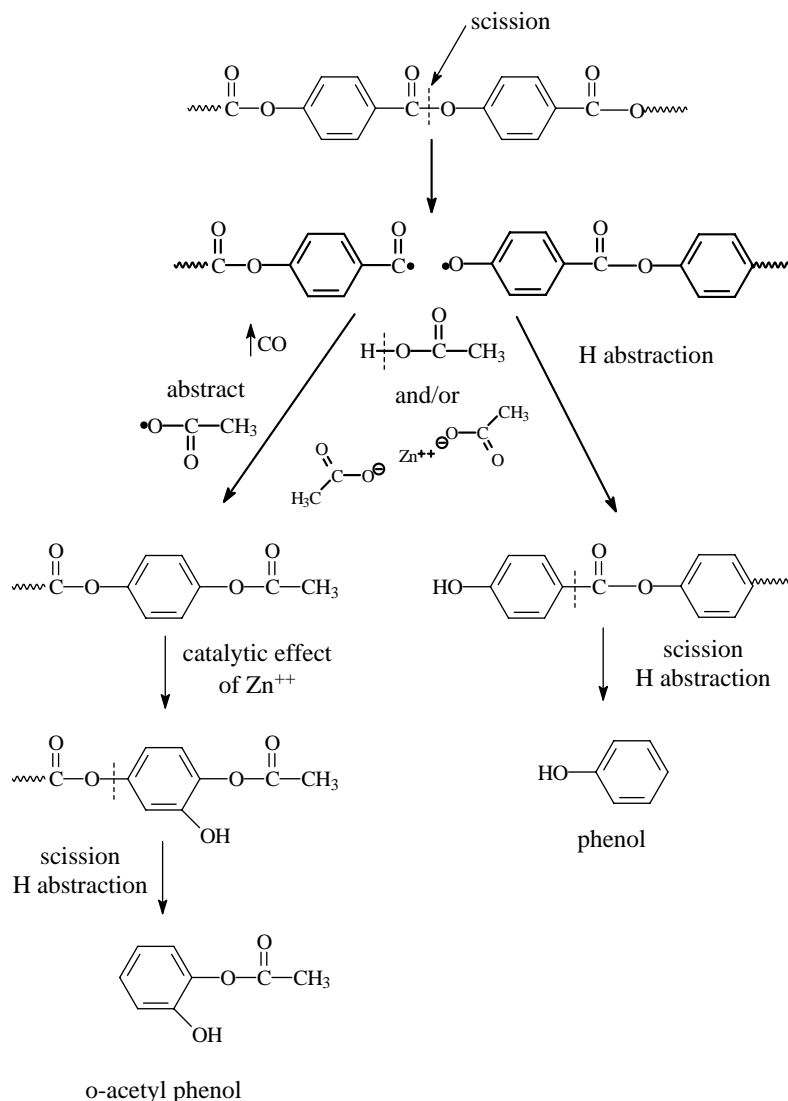


Fig. 13. Proposed mechanism of degradation process of the LCP in Zn-SPS/LCP blend: formation of *p*-acetyl phenol and phenol.

chain-ends, because that band was not present in the neat Zn-SPS with high residual ZnAc.

More discernable changes in the FTIR spectra for the blends were observed in the region of the C–C stretching of the benzoic or naphthanoic groups of the LCP, Fig. 14. The bands at 1414 and 1506 cm⁻¹ are due to skeletal vibrations of the benzoate and naphthanoate rings [28]. The peak at 1414 cm⁻¹ arises from the bonds adjacent to the –C(O)– of the ester group, and the 1506 cm⁻¹ absorption is due to the bonds adjacent to the –O– in the ester group. The peak at 1602 cm⁻¹ is due to the skeletal vibrations in the benzoate and naphthanoate rings for bonds not adjacent to the ester groups, and the bands at 1630 and 1472 cm⁻¹ arise from vibrations of bonds not adjacent to the ester groups in the naphthanoate ring.

The vibrations of the bonds adjacent to the ester groups (1414 and 1506 cm⁻¹) were perturbed by melt blending. For the 95/5 5.6Zn-SPS/LCP blend, those two absorptions disappeared, and new absorptions occurred at 1421 and 1518 cm⁻¹. That result can be explained with a similar explanation as for the changes in the carbonyl stretching. The

peak from the bonds adjacent to the –C(O) of the ester group in LCP may be perturbed by substitution of acetyl end groups for which the C–C stretching appears at 1430 cm⁻¹ [27], resulting in the shift of the peak from 1414 cm⁻¹ (LCP) to 1421 cm⁻¹ (blends). The shift of the absorption due to the bonds adjacent to the –O– in the ester group from 1506 cm⁻¹ (LCP) to 1518 cm⁻¹ (blends) may stem from the conjugation effect induced by the substitution of acetate end groups. The changes in C–C stretching for the 85/15 blend are quite similar to those for the 95/5 blend, except for the fact that the bands are broader than those for the 95/5 blend, which may again be due to the presence of both LCP agglomerates and nanoparticles.

The above explanation is further supported by the FTIR result for the 10.8Zn-SPS/LCP blends shown in Fig. 15. The morphology for those blends corresponds to a heterogeneous dispersion of large LCP domains and nanoparticles. For the 90/10 and 75/25 10.8Zn-SPS/LCP blends, all four absorptions, 1414, 1506, 1420, and 1518 cm⁻¹ were observed in the C–C stretching region, consistent with the two different particles seen in the morphology.

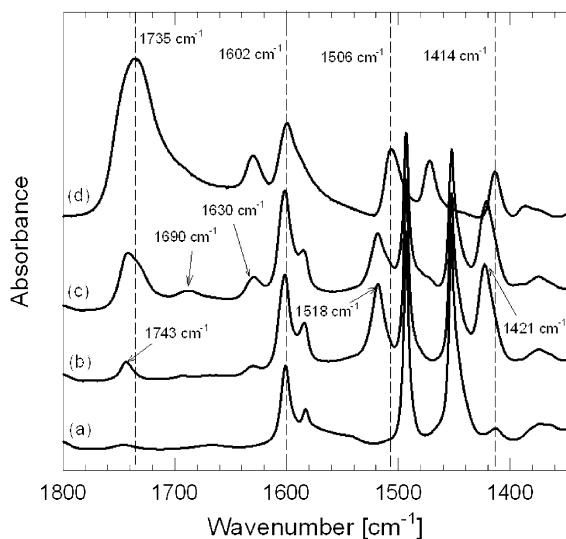


Fig. 14. FTIR spectra of the 5.6Zn-SPS/LCP blends and the neat polymers showing region of carbonyl stretching and carbon–carbon skeletal stretching; (a) 5.6Zn-SPS (b) 95/5 5.6Zn-SPS/LCP (c) 85/15 5.6Zn-SPS/LCP blend (d) LCP.

Although all four absorptions in the C–C stretching region were observed in the 90/10 and 75/25 blends, the shape of bands were quite different in the FTIR spectra for the two blends. The band at around 1421 cm^{-1} for the 90/10 10.8Zn-SPS blend was asymmetric in shape with higher intensity on the 1421 cm^{-1} side than at the 1414 cm^{-1} side. In contrast, the band for the 75/25 10.8Zn-SPS blend was also asymmetric, but with higher intensity on the 1414 cm^{-1} side, which corresponds to the band observed in the neat LCP. This, however, is consistent with the morphology of the two blends. In general, the 10.8Zn-SPS/LCP blends exhibited lower relative concentrations of nanoparticles and higher concentrations of larger LCP agglomerates as the LCP concentration increased in the blend. The fact that the 1414 and 1506 cm^{-1}

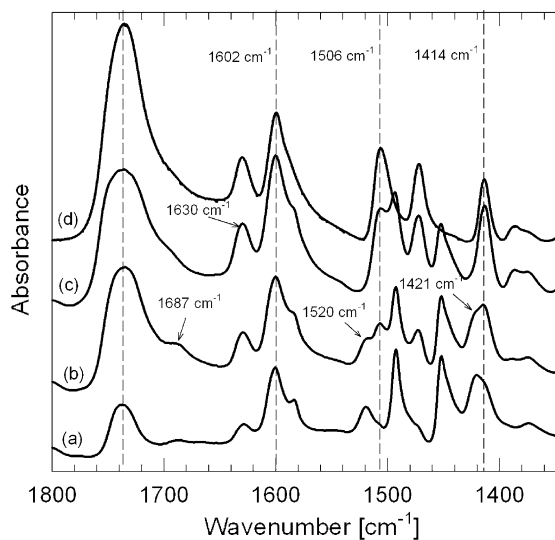


Fig. 15. FTIR spectra of the 10.8Zn-SPS/LCP blends and the neat LCP showing region of carbonyl stretching and carbon–carbon skeletal stretching; (a) 90/10 (b) 75/25 (c) 50/50 10.8Zn-SPS/LCP blend (d) LCP.

bands were absent in the 95/5 5.6Zn-SPS/LCP sample, where only nanoparticles were observed, and those bands persisted in the 90/10 and 75/25 10.8Zn-SPS/LCP samples, where both LCP agglomerates and nanoparticles existed, is consistent with the assignments of the 1414 cm^{-1} band being characteristic for the agglomerates and the 1421 cm^{-1} band indicative of the nanoparticles.

4. Conclusions

Nanoparticles were formed in situ during melt blending of an HBA/HNA LCP and zinc salts of sulfonated polystyrene ionomers at elevated temperatures due to a chemical reaction that involved the LCP and residual ZnAc from the neutralization of the ionomer. The size distribution and particle density of nanoparticles were affected by the LCP composition. An increase in the amount of the LCP led to a heterogeneous distribution of nanoparticles in both size and particle density, because of a lower degree of conversion of the LCP phase to nanoparticles. That may be due to a combination of insufficient ZnAc and/or the lower melt viscosity that occurs due to the presence of a macroscopic LCP phase.

The nanoparticles were crystalline, but the crystal structure did not correspond to that of either the parent LCP or homopolymers of the LCP components. The crystalline peaks in the WAXD patterns that arose from the nanoparticles persisted up to $350\text{ }^{\circ}\text{C}$, whereas the LCP crystallites melted at $\sim 280\text{ }^{\circ}\text{C}$. One explanation for the change in the crystal structure of the LCP-nanophase is the production of specific end-groups, e.g. phenyl acetate, and lower molecular weight that resulted from degradation of the LCP. Annealing temperature and time had a significant effect on the structural changes of the nanoparticles in the blends, whereas similar thermal treatment of the neat LCP and Zn-SPS did not induce any changes in their WAXD patterns.

Several volatiles other than the major degradation products from the neat polymers, i.e. phenol and styrene, were produced in the blends at elevated temperatures, including phenyl acetate, *o*-acetyl phenol, 4-hydroxybenzoic acid, and 3-phenyl furan. Small amounts of acetic acid were also found in both the neat Zn-SPS and blends. GC–MS results indicated that substantial chain scissions and end group modifications occurred by the reaction of the LCP with ZnAc and/or acetic acid at elevated temperatures. Based on the detected volatiles, a degradation mechanism of the LCP in the presence of ZnAc and/or acetic acid in the Zn-SPS/LCP blend was proposed.

FTIR analysis confirmed the chain modification of the LCP, specifically, the development of phenyl acetate chain ends on the LCP. The changes in the FTIR spectra were consistent with the evolution of morphology of the blend, indicating that the formation of nanoparticles followed the modification of the chain ends of LCP.

Acknowledgements

This work was supported by a grant from the Polymer Program of the National Science Foundation (DMR 0303696).

The synchrotron SAXS experiments were carried out in the National Synchrotron Light Source, Brookhaven National Laboratory, supported by the DOE.

References

- [1] Lee HS, Fishman D, Kim B, Weiss RA. *Polymer* 2004;45:7807–11.
- [2] Makowski HS, Lundberg RD, Singhal GH. US Patent 3870841; 1975.
- [3] Weiss RA, Lundberg RD, Turner SR. *J Polym Sci, Polym Chem Ed* 1985; 23:549.
- [4] Weiss RA, Huh W, Nicolais L. *Polym Eng Sci* 1987;27:684.
- [5] Lieser GJ. *J Polym Sci, Polym Phys Ed* 1983;21:1611.
- [6] Yoon DY, Masciocchi N, Depero LE, Viney C, Parrish W. *Macromolecules* 1990;23:1793.
- [7] Iannelli P, Yoon DY, Parrish W. *Macromolecules* 1994;27:3295.
- [8] Gutierrez GA, Chivers RA, Blackwell J, Stamatoff JB, Yoon H. *Polymer* 1983;24:937.
- [9] Kaito A, Kyotani M, Nakayama K. *Macromolecules* 1990;23:1035.
- [10] Wilson DT, Vonk CG, Windle AH. *Polymer* 1993;34:227.
- [11] Sun Z, Cheng H-M, Blackwell J. *Macromolecules* 1991;24:4162.
- [12] Romo-Urbe A, Windle AH. *Macromolecules* 1996;29:6246.
- [13] Hanna S, Windle AH. *Polymer* 1992;33:2825.
- [14] Xu L. PhD Thesis, University of Connecticut; 2003.
- [15] Jiang DD, Yao Q, McKinney MA, Wilkie CA. *Polym Degrad Stab* 1999; 63:423.
- [16] Naffakh M, Ellis G, Gomez MA, Marco C. *Polym Degrad Stab* 1999; 66:405.
- [17] Hummel DO, Neuhoff U, Bretz A, Duessel HJ. *Makromol Chem* 1993; 194:1545.
- [18] Campoy I, Gomez MA, Marco C. *J Therm Anal Calorim* 1998;52:705.
- [19] Campoy I, Gomez MA, Marco C. *Polymer* 1998;39:6279.
- [20] Xu L, Weiss RA. *Polym Degrad Stab* 2004;84:295.
- [21] Otton J, Rattou S, Vasnev VA, Markova GD, Nametov KM, Bakhmutov VI, et al. *J Polym Sci, Part A: Polym Chem* 1988;26:2199.
- [22] Otton J, Rattou S. *J Polym Sci, Polym Chem* 1989;27:3535.
- [23] Ignatov VN, Carraro C, Tartari V, Pippa R, Scapin M, Pilati F, et al. *Polymer* 1997;38:201.
- [24] Sueoka K, Nagata M, Ohtani H, Naga N, Tsuge S. *J Polym Sci, Part A: Polym Chem* 1991;29:1903.
- [25] Jin X, Chung T-S. *J Appl Polym Sci* 1999;73:2195.
- [26] Moghaddam FM, Ghaffarzadeh M, Abdi-Oskoui SH. *J Chem Res Synop* 1999;(9):574.
- [27] Colthup NB, Daly LH, Wiberley SE. *Introduction to infrared and Raman spectroscopy*. 3rd ed. New York: Academic; 1990.
- [28] Ouchi I, Hosoi M, Shimotsuma S. *J Appl Polym Sci* 1977;21:3445.